AD-A069 284 BELL AEROSPACE TEXTRON BUFFALO N Y F/G 20/5
VISIBLE CHEMICAL LASER DEVELOPMENT.(U)
MAY 79 J A BLAUER, W F BRANDKAMP, W C SOLOMON DASG60-78-C-0030

UNCLASSIFIED NL

1 OF 1
AD
A069284

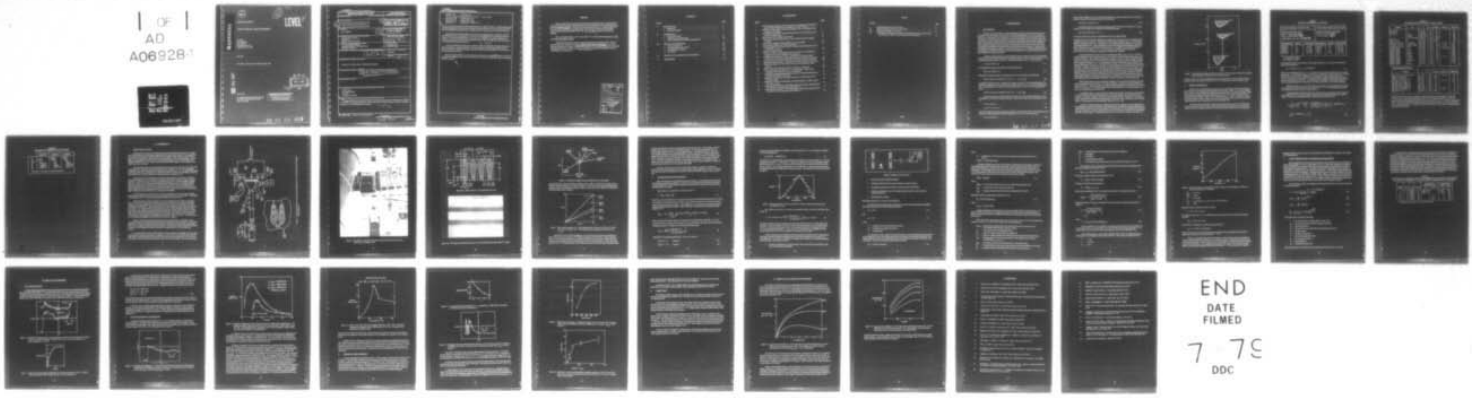

END
DATE
FILMED
7 79
DDC


1·0
1·1
1·25
1·4
1·6
1·8
2·0
2·2
2·5
2·8
3·15
3·5
4·0
4·5
NATIONAL BUREAU OF STANDARDS
MICROCOPY RESOLUTION TEST CHART

LEVEL II

TECHNICAL REPORT

VISIBLE CHEMICAL LASER DEVELOPMENT

J.A. Blauer
W.F. Brandkamp
W.C. Solomon
Bell Aerospace Textron
Buffalo, New York 14240

May 1979

Final Report for Period January 1978 to December 1978

Prepared For

U.S. ARMY BALLISTIC MISSILE DEFENSE
ADVANCED TECHNOLOGY CENTER
Huntsville, Alabama

Unclassified

SECURITY CLASSIFICATION OF THIS PAGE (*When Data Entered*)

REPORT DOCUMENTATION PAGE

READ INSTRUCTIONS BEFORE COMPLETING FORM

1. REPORT NUMBER

2. GOVT ACCESSION NO.

3. RECIPIENT'S CATALOG NUMBER

4. TITLE (*and Subtitle*)

(6) Visible Chemical Laser Development.

(9) 5. TYPE OF REPORT & PERIOD COVERED

Final Technical Report • Jan [illegible] - Dec [illegible]78

6. PERFORMING ORG. REPORT NUMBER

7. AUTHOR(s)

Jay A. Blauer

(15) 8. CONTRACT OR GRANT NUMBER(s)

DASG60-78-C-0030

9. PERFORMING ORGANIZATION NAME AND ADDRESS

Bell Aerospace Textron
P.O. Box 1
Buffalo, New York 14240

10. PROGRAM ELEMENT, PROJECT, TASK AREA & WORK UNIT NUMBERS

(11) May 79

11. CONTROLLING OFFICE NAME AND ADDRESS

U.S. Army Ballistic Missile
Defense, Advanced Technology Center,
Huntsville, Alabama

12. REPORT DATE

31 January 1979

13. NUMBER OF PAGES

14. MONITORING AGENCY NAME & ADDRESS (*if different from Controlling Office*)

(12) 37p.

15. SECURITY CLASS. (*of this report*)

Unclassified

15a. DECLASSIFICATION/DOWNGRADING SCHEDULE

N/A

16. DISTRIBUTION STATEMENT (*of this Report*)

Approved for Public Release, Distribution Unlimited

17. DISTRIBUTION STATEMENT (*of the abstr*

(10) Jay A./Blauer, Warren F./Brandkamp
Wayne C./Solomon

18. SUPPLEMENTARY NOTES

19. KEY WORDS (*Continue on reverse side if necessary and identify by block number*)

Visible Laser
Chemical Pumping
Tin Oxide
Electronic Excitation

20. ABSTRACT (*Continue on reverse side if necessary and identify by block number*)

Experimental data are presented relative to attempts to induce laser oscillations in the vicinity of 5578 Å in a chemically prepared tin oxide medium. The chemical system of interest is partially described by the following series of reactions:

→ next page

DD FORM 1 JAN 73 1473 EDITION OF 1 NOV 65 IS OBSOLETE

Unclassified

SECURITY CLASSIFICATION OF THIS PAGE (*When Data Entered*)

408 855

$Sn\ (^3P_0) + M = Sn\ (^3P_1) + M$
$Sn\ (^3P_1) + N_2O\ (^1\Sigma^+) = SnO\ (X^1\Sigma^+, a^3\Sigma^+, b^3\pi, \ldots) + N_2\ (^1\Sigma^+ g)$
$SnO\ (a^3\Sigma^+) + M = SnO\ (X^1\Sigma^+) + M$
$SnO\ (b^3\pi) + M = SnO\ (X^1\Sigma^+, a^3\Sigma^+)$
$SnO\ (a^3\Sigma^+) = SnO\ (X^1\Sigma^+) + 20622\ cm^{-1}$

Atomic tin was first prepared by shock-heating mixtures of $SnCl_4$ in Argon. The plenum gases were accelerated through a nozzle bank and molecular N_2O was injected into the supersonic flow stream. Medium diagnostics were conducted in a windowed section downstream of the nozzle exit plane.

During the course of these studies, it was found that atomic chlorine, a fragament of $SnCl_4$ dissociation, proved very deleterious to the retention of SnO ($a^3\Sigma^+$) excited molecules within the medium. To overcome this difficulty, the tin vapor was prepared by entraining within the oncoming shock wave the products of an exploding tin wire. This permitted over a 100 fold increase in the concentration of excited species.

a3 Sigma(+)

To date, all attempts to induce laser oscillations within the chemically prepared medium have been unsuccessful. Computer modeling of the system indicates that the major reasons for this failure were that the medium temperature was far too high, and that the density of tin vapor must be increased about three fold.

Data are presented relative to number density measurements for SnO ($a^3\Sigma^+$) under a variety of experimental conditions and to the several attempts to induce laser oscillations within the seemingly optimized medium.

PREFACE

The work described in this Technical Report was accomplished under the sponsorship of the United States Army Ballistic Missile Defense Advanced Technology Center (BMDATC) under Contract DASG60-78-C-0030. The project has been monitored by Dr. E.E. Sanman (BMDATC). The work was accomplished at the High Energy Laser Research Facilities of Bell Aerospace Textron (BAT) located near Buffalo, New York. Dr. Jay A. Blauer of BAT was the Project Manager.

The work reported herein covers a time period of 12 months begining in January of 1978 and ending in December of 1978.

The facilities and all test equipment described herein were furnished by BAT. The test data described were obtained by Dr. Jay A. Blauer and Mr. Warren F. Brandkamp. The report itself was authored by Dr. Blauer. Special thanks are given to Dr. Eugene Sanman who encouraged the beginning of this work and to Dr. Wayne C. Solomon who aided in the interpretation and initial design of the experiment.

CONTENTS

ILLUSTRATIONS

TABLES

I. INTRODUCTION

1. BACKGROUND

Success in the development of a visible chemical laser must rest ultimately upon our understanding of those phenomena which give rise to visible chemiluminescence. It is not surprising, therefore, that much attention has been paid to the detailed chemistry and physics of several candidate systems. Nevertheless, laser oscillation at visible wavelengths has yet to be demonstrated for a purely chemical system. Major problems encountered in this regard include the short radiative lifetimes of typical electronically excited states, the usually unfavorable branching ratios associated with exothermic reactions which can produce electronically excited species, and the rather broad and unselective distribution of vibration-rotation states within an electronic state. Since most of the exothermic reactions of interest are of the atom-molecule type, one additional problem involves the development of reliable techniques for reactive atom generation at number densities which are large enough to be of practical interest.

A vigorous research effort in several laboratories has been directed toward the measurement of photon yields and radiative lifetimes for seemingly promising candidate molecular systems [1-16]. The reported photon yields vary from 10^{-5} reported by Eckstrom et al. [1] for the reaction

$$Ti + N_2O = TiO^{\ddagger} + N_2 \qquad \text{(i)}$$

to 0.64 reported by these same authors for the following system:

$$Sm + N_2O = SmO^{\ddagger} + N_2 \qquad \text{(ii)}$$

Other values of interest include a branching ratio of 0.51 for the following combination:

$$Sn(^3P) + N_2O(^1\Sigma) = SnO(X^1\Sigma^+, a^3\Sigma^+, b^3\pi. \ldots) + N_2\,(^1\Sigma_g^+) \qquad \text{(iii)}$$

as reported by Felder et al. [3]. Linevsky et al. report a value of 0.7 for this branching ratio. The somewhat analogous system involving the GeO molecule has proven to be much less promising however. Thus, Capelle et al. [17] report a quantum yield of Φ (a) $\sim 6.8 \times 10^{-4}$ for the following reaction:

$$Ge(^3P) + N_2O(^1\Sigma) = GeO(X^1\Sigma^+, a^3\Sigma^+, b^3\pi, \ldots) + N_2\,(^1\Sigma_g^+) \qquad \text{(iv)}$$

While these reactions involve single-step excitation (primary processes), Polanyi et al. [10] investigated a novel system involving excitation by means of an energy transfer (secondary process), i.e.,

$$H + HI = H_2(v) + I \qquad \text{(v)}$$

$$H_2(v) + I = H_2(v\text{-}2) + I^* \qquad \text{(vi)}$$

We have investigated the lasing potential of a variation of this system in detail. The variation involves the in-situ chemical generation of atomic hydrogen by means of the following process:

$$Na + HI = NaI + H \qquad \text{(vii)}$$

In like manner, McDermot et al. [18] have recently shown a somewhat similar system, involving the transfer of energy from chemically formed O_2 ($^1\Delta g$) to lase.

$$O_2(^1\Delta g) + I = O_2(^3\Sigma_u^-) + I^* \qquad \text{(viii)}$$

Of particular interest to the present proposed research is the work of Fontijn et al. [3] and Linevsky et al. [4] relative to the kinetics of the following process:

$$Sn + N_2O = SnO(X^1\Sigma^+, A^1\pi, \ldots) \qquad \text{(ix)}$$

The results of these two studies are reproduced in Table I for easy reference.

Linevsky et al. [4] further report that $Sn(^3P_1)$ reacts with N_2O about a factor of 25 faster than do ground state atoms, i.e., $Sn(^3P_0)$. The results of Fontijn agree to within a factor of 2 of this result. Finally, of particular interest to us, Linevsky et al. [4] placed their flame intracavity to a dye laser containing Rhodamine 6G. They examined the output of the laser spectroscopically and found no gain or absorption in the appropriate spectral region for a $\rightarrow$ X radiation. Since the sensivitivy of this technique is quite high, ca. 10^{-4} cm^{-1}, they conclude that their number densities for SnO, ca.$> 10^{13}$/cc, are far below that required to achieve laser threshold.

The radiative lifetime of the $a^3\Sigma^+$ state was reported by Mayer et al. [7] to be $\sim$ 333 μsec. Another important feature of these systems is to be found from their potential energy curves. Thus, for SnO, see Figure 1, the equilibrium internuclear separation of the $a^3\Sigma^+$ state is noticeably larger than that for the ground state. The Franck-Condon principle requires that the most likely transition will be vertically downward [19]. As a consequence, the lower level reached will not likely be the ground vibrational level but a state for which $\nu'' \geq 3$ depending upon the initial vibrational state within the $a^3\Sigma^+$ manifold. Furthermore, since the vibrational spacing in the $X^1\Sigma^+$ state is only 822.9 cm^{-1}, the theory of vibrational relaxation [20] assures us that equilibration within the ground state manifold will be rapid. As a consequence, the terminal state of the radiative process will be collisionally depleted. This is just the situation desired for efficient laser action. Finally, another factor which favors a high branching ratio for reactions (iii) and (iv) into the $SnO(a^3\Sigma^+)$ product state is that it is spin allowed, whereas, branching into the ground state is forbidden. Of course, for heavy molecules like SnO, this spin rule is not rigorous, otherwise, no ground state product would result at all.

Before these systems can be successfully investigated, the rather difficult problem of reactive metal atom generation must be solved. For research purposes, we require a metal atom density in excess of $10^{15}/cm^3$. This is more than two orders of magnitude larger than that achieved by Linevsky et al. [4] or Felder et al. [3] in their respective flow tube experiments. For research purposes, our solution to this problem has been two-fold.

In the first instance, we have shock-heated binary mixes of $SnCl_4$ and Argon to temperatures in excess of 6000°K to affect total dissociation. The hot plenum gases were then cooled to near 1000°K by acceleration through a nozzle into the observation chamber. Gaseous N_2O was injected into the supersonic flow field near the trailing edge of the nozzle. The observations to date consisted chiefly of a measurement of chemiluminescent intensity at 5544 ± 50Å.

In order to avoid the presence of undesirable dissociation fragments, we have sought an alternate versatile and reproducible approach for introducing pure tin vapor into the argon gas plenum. To accomplish this, we place a thin tin wire parallel to the nozzle and one inch upstream into the plenum. The wire is exploded (by electric discharge) 5 μsec before its position is traversed by the approaching incident wave (pure argon). The limiting features now are to be traced to the size of the wire and

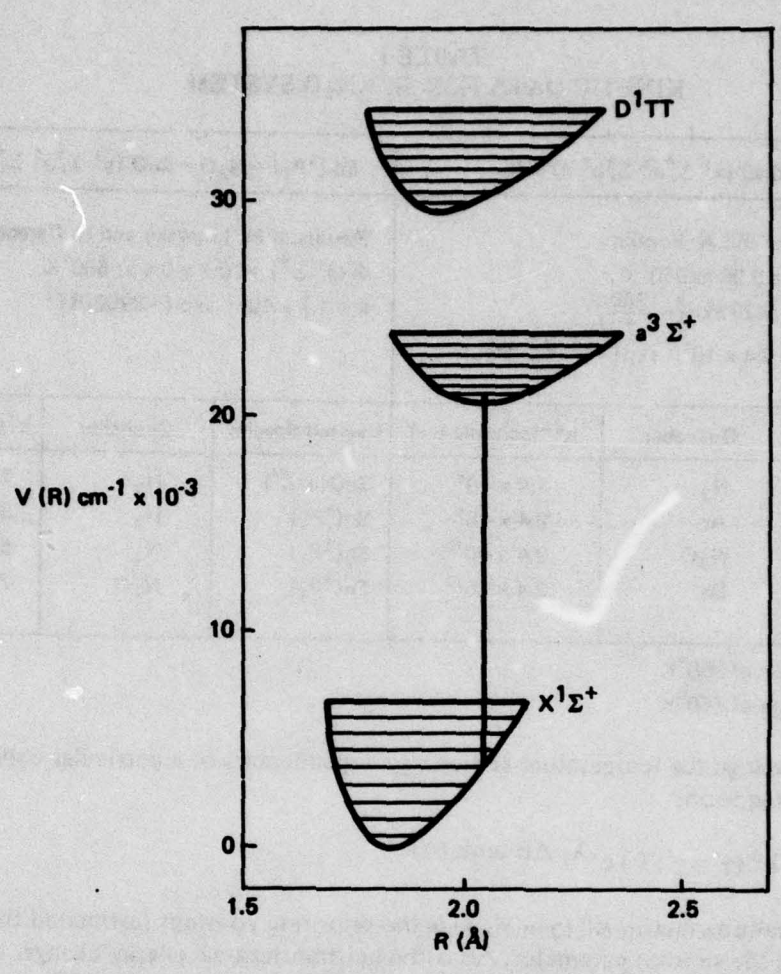

Figure 1. Potential Energy Diagram of SnO According to the Tabulations of Suchard [7] and the Spectral Parameters of Linevsky [4] for the $a^3\Sigma$ State

the input energy. The number densities achieved are approaching the range of interest. This approach is a variation of that used by Blair et al. [21] in their studies of metal oxidation lasers.

2. MODEL DEVELOPMENT

There has been a substantial improvement in our understanding of the physics and chemistry of the Sn - N_2O chemical system during the past two years. Felder et al. [3] have published a very extensive report detailing their findings and reinterpreting their experimental results. When these results are integrated with the findings of Linevsky et al. [4] a fairly complete picture of the relevant kinetics appears. Most of the information needed to construct a computer model of the system is given in Table I. Other recent results of importance to the construction of a viable model include the data of Wiesenfeld et al. [22] and Capelle [23].

Since much of the information regarding deactivational processes of Sn and SnO species refers to a single temperature, we have utilized the information (suprisal) theory as outlined by Levine et al. [24] to develop estimates of the required functional dependence where applicable.

TABLE I
KINETIC DATA FOR $Sn + N_2O$ SYSTEM

$Sn\ (^3P_0) + N_2O = SnO\ (x^1\Sigma^+, a^3\Sigma^+, b^3\pi) + N_2$			$Sn\ (^3P_1) + N_2O = SnO\ (x^1\Sigma^+, a^3\Sigma^+, b^3\pi) + N_2$		
Results of W. Felder and A. Fontijn $\Phi\ (a^3\Sigma^+) = 0.53 \pm 0.26$ at 950°K $\Phi\ (b^3\pi) = (0.59 \pm 0.29 \exp\left(-\frac{1200}{T}\right)$ $k\ (330° - 950°K) = 5.4 \times 10^{11} \exp\left(-\frac{4490 \pm 360}{T}\right)$			Results of M. Linevsky and R. Carabetta $\Phi\ (a^3\Sigma^+) = 0.7 \pm 0.4$ at 550°K $k = 1.7 \times 10^{13} \exp(-3950/RT)$		
Excited Species	**Quencher**	**k**(cc/mole-sec)**	**Excited Species**	**Quencher**	**k‡(cc/mole-sec)**
$SnO(a^3\Sigma^+)$	N_2	1.4×10^8	$SnO(a^3\Sigma^+)$	H_2	2.0×10^{11}
$SnO(a^3\Sigma^+)$	Ar	2.4×10^8	$Sn(^3P_1)$	H_2	3.0×10^{12}
$SnO(a^3\Sigma^+)$	N_2O	2.4×10^{10}	$Sn(^3P_1)$	N_2	5.4×10^{11}
$SnO(a^3\Sigma^+)$	Sn	2.4×10^{12}	$Sn(^3P_1)$	N_2O	7.8×10^{11}

** At a temperature of 950°K

‡ At a temperature of 550°K

This approach develops the temperature and energy dependencies of a particular collisional process in the following form:

$$k = e^{-\lambda_0} k^0 (\gamma \rightarrow \gamma'; T)\, e^{-\lambda_1 \Delta E \tanh(\Delta)} \qquad (x)$$

Here λ_0 is a normalizing factor, $k^0 (\gamma \rightarrow \gamma'; T)$ is the prior rate constant (estimated from molecular parameters), λ_1 is the suprisal parameter, ΔE is the net translational energy change, and $\Delta = \Delta E/2kT$. The value of λ_0 results from a comparison to the estimated two-body collision frequency for $\Delta E = 0$. The value of λ_1 results from a comparison of the normalized function with experimental data for a well-characterized system. As more data become available, it is possible to describe λ_1 with ever improved precision. This reduces the entropy (uncertainty) of the model developed.

Finally, estimates of the rates for recombinative and other exchange (metathesis) reactions were obtained from well documented theoretical sources [25-27]. The resulting kinetics model of the chemically reactive system is found in Table II.

Inversion densities developed between the electronic states of moderately heavy molecular species will tend to be low due to extensive rotational and vibrational dilution of the excitation energy. For tin oxide or germanium sulfide, the gain equation is given by [30].

$$a = \frac{\beta}{4(2\pi)^{3/2}} \left(\frac{m}{kT}\right)^{1/2} \frac{S(J', J'')}{\tau \omega^3} \left[\frac{R_e^2(r) q(v', v'')}{\Sigma_{v''} R_e^2(r)\, q(v', v'')}\right] \left\{\frac{1}{2J'+1} [SnO(a^3\Sigma^+)]_{v', J''} - \frac{3}{2J''+1} [SnO(X^1\Sigma^+)]_{v'', J''}\right\} \qquad (xi)$$

TABLE II
REACTION RATE DATA FOR THE Sn-N_2O SYSTEM

Reaction	M	A	N	E(Kcal)	Comments	References
$Sn + O = SnO$	*	5.2×10^{18}	-1.0	0.0		25
$Sn + Sn = Sn_2$	*	1.7×10^{19}	-1.0	0.0		25
$O + O = O_2$	Ar, He	1.89×10^{13}	0.0	-1.7		28
	ϕ_2, 28ϕ	1.38×10^{18}	-1.0	0.34		28
	N_2, 1.7 N_2O, SnO	1.78×10^{17}	-1.0	-0.45		28
$N_2O = N_2 + O$	*	5.0×10^{14}	0.0	57.6		28
$SnO_2 = Sn + O$	*	1.4×10^{16}	0.0	116.3		26
$Sn\ (^3P_{J+1}) = Sn\ (^3P_J)$	N_2O, SnO_2	5.4×10^{12}	0.0	1.4	J = 1, 0	4, 24
$Sn\ (^3P_{J+1}) = Sn\ (^3P_J)$	N_2, Sn, O, SNO	7.9×10^{-4}	5.0	-2.84	J = 1, 0	4, 24
$Sn\ (^3P_{J+1}) = Sn\ (^3P_J)$	Ar, He	5.8×10^{-8}	6.0	-2.0	J = 1, 0	4, 29
SnO(a) = SnO(x)	N_2	1.2×10^{-2}	4.0	7.2	$a^3\Sigma^+$, $X^1\Sigma^+$	3, 24
SnO(a) = SnO(x)	Ar, He	1.6×10^{-2}	4.0	6.8		3, 24
SnO(a) = SnO(x)	N_2O	3.7×10^{2}	3.0	4.3		3, 24
SnO(a) = SnO(x)	Sn, SnO	3.9×10^{8}	1.5	2.6		3, 24
SnO(a) = SnO(x)	SnO_2	1.0×10^{13}	0.5	0.0		3, 24
SnO(b) = SnO(a)	N_2, SnO	1.5×10^{3}	2.5	8.6	$b^3\pi$, $a'^1\Sigma^+$	3, 24
SnO(b) = SnO(a)	Ar, He	2.6×10^{-9}	6.0	4.3		3, 24
SnO(b) = SnO(a)	N_2O, SnO_2	2.7×10^{-1}	4.0	1.9		3, 24
SnO(b) = SnO(a)	Sn	1.1×10^{7}	2.0	0.7		3, 24
SnO(a) = SnO(x)	Photon	3.0×10^{3}	0.0			7

Pumping and Exchange Reactions

Reaction	A	N	E(Kcal)	Comments	References
$SnO_2 + Sn\ (^3P_J) = SnO(x) + SnO(x)$	4.4×10^{13}	0.0	5.5	J = 2, 1, 0	27
$SnO_2 + O = SnO(x) + O_2$	2.8×10^{13}	0.0	10.0		27
$SnO\ (a,x) + N_2O = SnO_2 + N_2$	3.9×10^{12}	0.0	17.0		27
$Sn\ (^3P_J) + O_2 = SnO(x) + O$	4.2×10^{13}	0.0	1.4	J = 2, 1, 0	3, 27
$Sn\ (^3P_0) + N_2O = SnO(x) + N_2$	1.6×10^{11}	0.0	4.5		3
$Sn\ (^3P_0) + N_2O = SnO(a) + N_2$	2.9×10^{11}	0.0	4.5		3
$Sn\ (^3P_0) + N_2O = SnO(b) + N_2$	9.6×10^{10}	0.0	4.5		3
$Sn\ (^3P_J) + N_2O = SnO(x) + N_2$	0.51×10^{13}	0.0	4.0	J = 2, 1	4
$Sn\ (^3P_J) + N_2O = SnO(a) + N_2$	1.18×10^{13}	0.0	4.0	J = 2, 1	4
$N_2O + O = N_2 + O_2$	2.0×10^{14}	0.0	28.0		28

Here β is the fractional isotopic abundance of the particular Sn isotope considered. In this case $\beta \sim 0.33$. Also, m is the mass of the molecule, $S(J', J'')$ is the Honl-London factor ($\sim J'$), ω is the wavenumber of the transition, Re(r) is the electronic moment, and $q(v', v'')$ is the Franck-Condon factor. For the case of SnO, the quantity in brackets is approximately 0.2, see ref [30]. The lifetime, τ, is taken as 333 μsec. The molecular constants required to compute species number densities are tabulated in Table III.

TABLE III
MOLECULAR CONSTANTS‡ FOR TIN OXIDE

	SnO($X^1\Sigma^+$)	SnO($a^3\Sigma^+$)	SnO($D^1\pi$)
Te	0	20622.0	29505.1
ωe	822.4	500.2	582.6
ωeXe	8.73	1.03	3.08
Be	0.3557190	0.28	0.314475
α_e	0.0021429	0.00086	0.00031455
D_e	0.2662×10^{-6}	0.351×10^{-6}	0.25×10^{-6}

‡Units of cm^{-1} after Fontijn et al [30] and Suchard [7].

II. EXPERIMENTAL

1. SHOCK-TUBE FACILITY

Since the reaction system of interest requires substantial quantities of atomic tin, we have spent considerable time in developing a reliable source for experimental purposes. Two approaches to a solution of this problem have been followed in this research. First, binary mixes of $SnCl_4$ in argon were shock-heated to temperatures in excess of 6000°K to affect total dissociation. The hot gaseous plenum behind the reflected wave was expanded through a nozzle to a final state in the vicinity of 1000°K and 10 torr. Gaseous N_2O was injected supersonically into the supersonic flow field at the nozzle exit plane.

The second approach involved the central placement of a thin wire of pure tin (0.25 mm dia) 2.5 cm upstream of the subsonic portion of the nozzle and parallel to it. The wire is discharged (exploded) 5 μsec before its position is traversed by the incident shock front. The gaseous Sn formed is entrained in the shock treated gases in a reproducible manner without the introduction of dissociation by-products. Typically, 800 joules of energy are used to explode the wire.

The shock-tube is of stainless steel and has an inside diameter of 6-3/8 inches. The driver has an inside diameter of 3-1/2 inches and is connected to the driven section by means of a conical transition. The driver and driven sections are separated by means of a double diaphragm arrangement. By careful control of the pressure within the interdiaphragm section, it proved possible to initiate the shock front to within 0.3 sec of the desired time. The driven section itself was 20 ft long and was interfaced to the reaction and observation chamber by means of a constant area duct which changed the cross-sectional geometry from 6-3/8 inch circular to 2.66 inch x 12.0 inch rectangular. This permits the development of 12 inches of active medium.

The test section has a cross section of 1.0 inch x 12.0 inch and is 9 inches long. Sapphire windows permit viewing of the first 6 inch of flow measured from the nozzle exit plane. A schematic of the apparatus and an accompanying photograph are given in Figures 2 and 3.

The nozzle array consists of a double row, the individual elements of which are described here. There are 95 primary nozzles in each row and each is flanked on its two sides by secondary nozzles. The primary nozzles have 0.052 inch diameter circular throats and 0.080 x 0.195 inch rectangular exit dimensions. The overall length of an element (leading from the shock tube plenum) is 0.320 inch. The subsonic portion of each element is a 60° conical convergent section of 0.070 inch length. The secondary nozzles are simple wedges having rectangular throats of 0.010 x 0.390 inch cross sections and exit dimensions of 0.035 x 0.390 inch. The secondary nozzles are provided with a common feed which was incorporated within the body of the nozzle array and consists of two channels 12 inches long and of rectangular cross section, 0.188 x 0.173 inch. A schematic and an accompanying photograph of the nozzle array are shown in Figure 4.

Before a shock tube nozzle beam apparatus is used to gather data, it is necessary to pay meticulous attention to the start-up transient phenomena associated with its operation. This becomes especially true when it is realized that for an improperly designed system the transient phenomena may never be completed during the achievable test time. The start-up transient can best be described in terms of a wave diagram for events occurring in the neighborhood of the nozzle plate, see Figure 5.

An analysis of these events, which is based upon the procedures of Rudinger [31], and which utilizes dynamic pressure measurements in regions 1, 2, and 5, reveals that the Q-shock will pass the observation point approximately 50 μsec after shock reflection at the nozzle plate. Since two complete regions (4 and 6) must pass the window in this time, the test condition will show an initial very

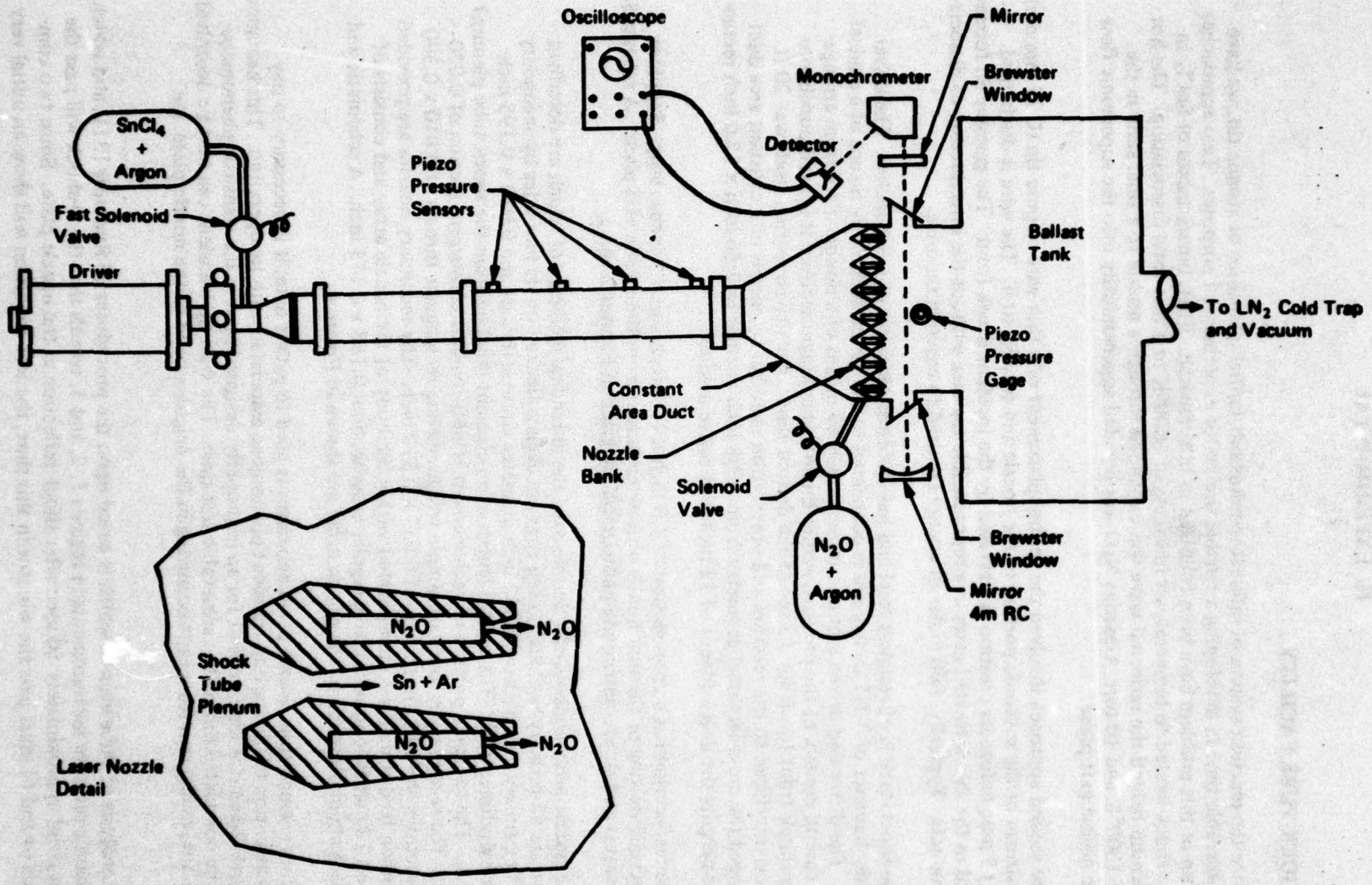

Figure 2. Schematic of Shock-Tube Laser Nozzle Apparatus with 12-Inch Optical Path Through Active Medium

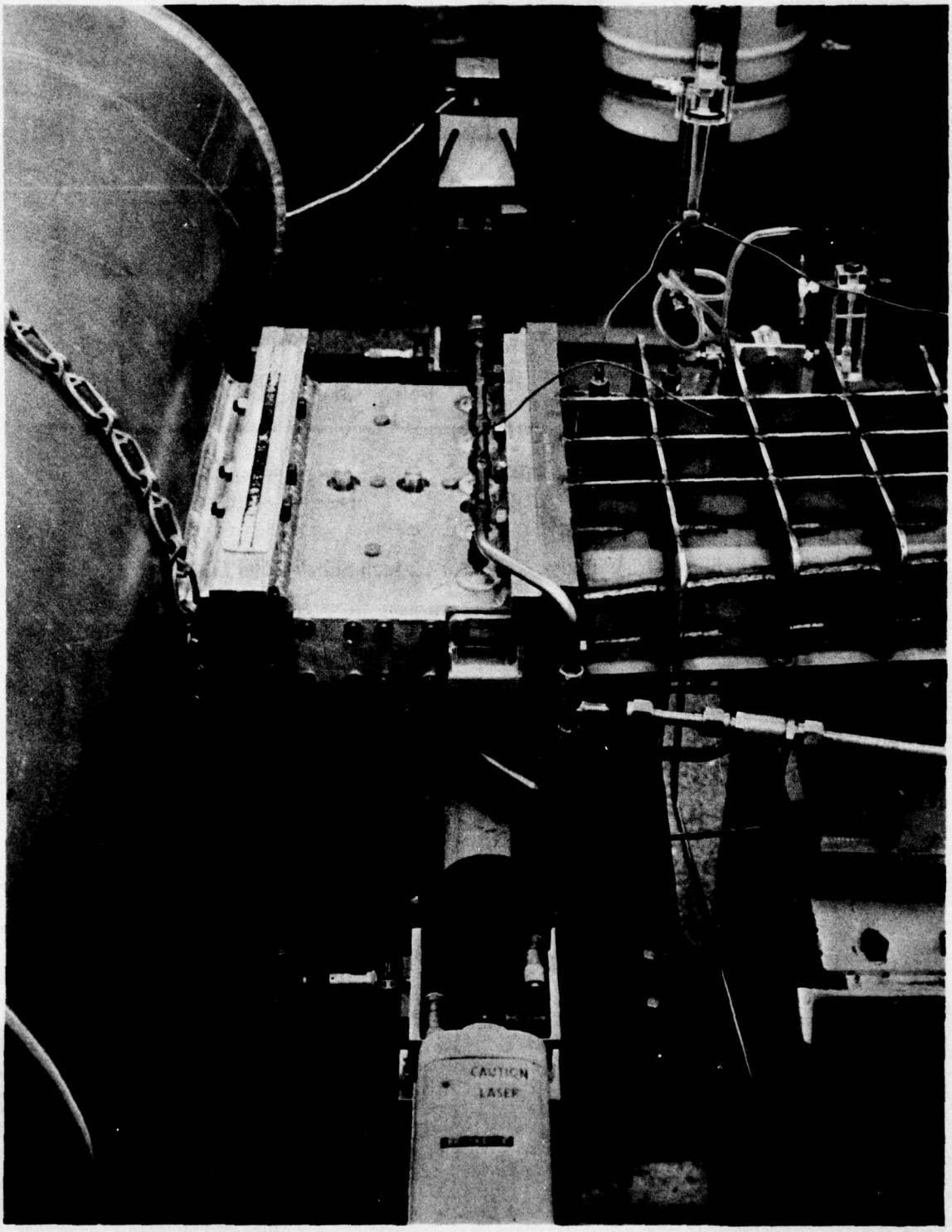

Figure 3. Photograph of Assembled Apparatus Showing the Constant Area Duct, Laser Cavity, and Ballast Tank

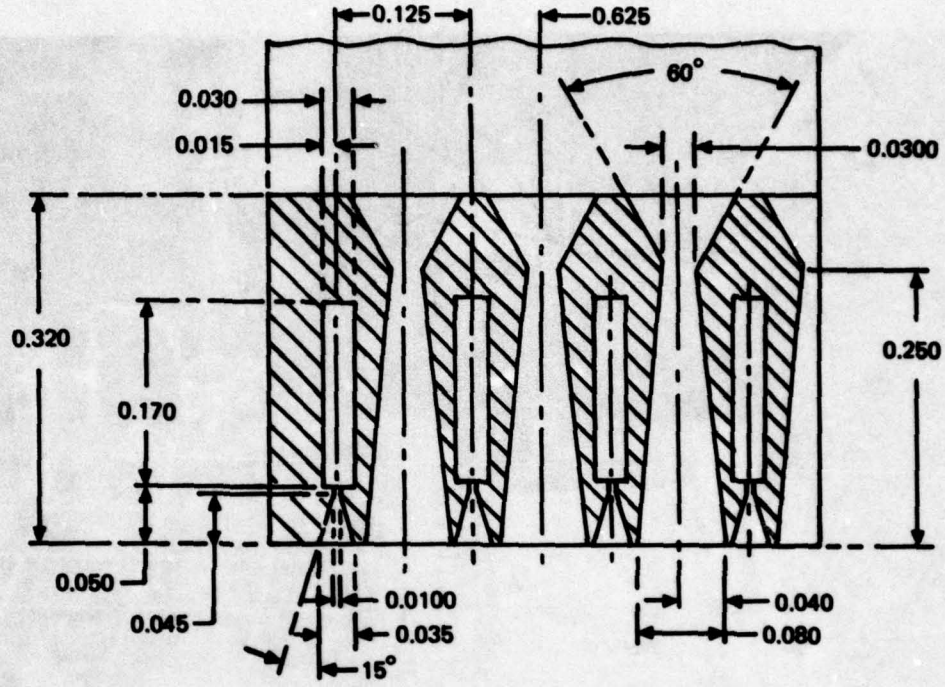

Figure 4(a). Body Nozzle for 12-Inch Shock-Tube Laser

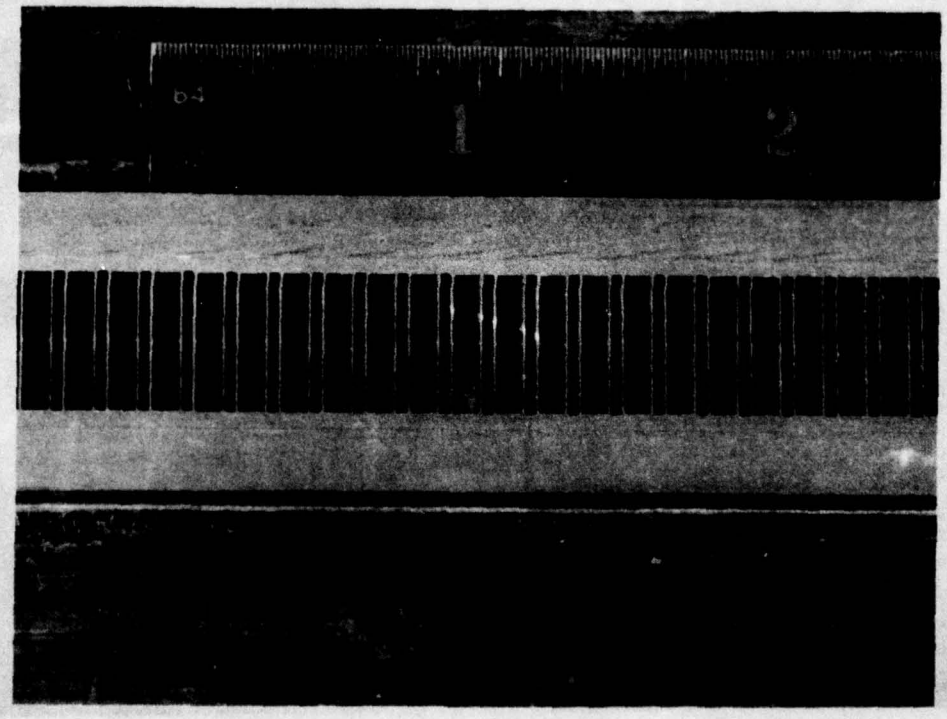

Figure 4(b). Photograph of Mixing Nozzle Array (2-1/2-Inch Section) Overall Length is 12 Inches

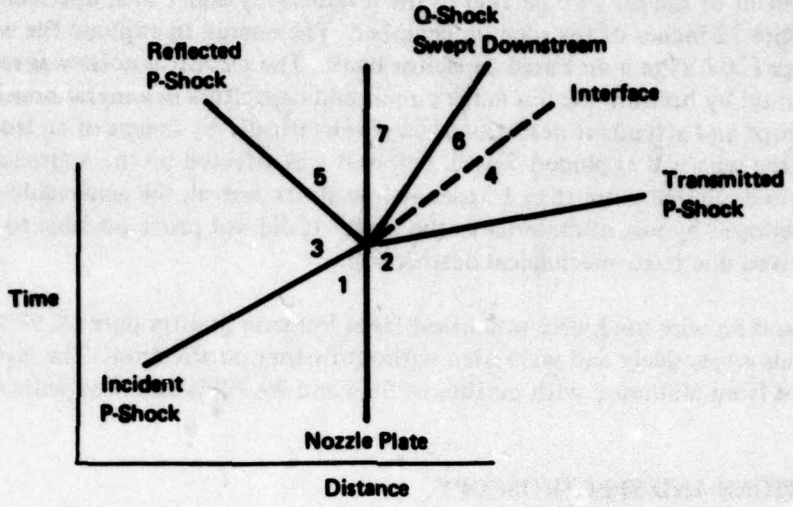

Figure 5. Typical Wave Diagram for Shock Reflection at a Nozzle Plate

unsteady behavior. Once the Q-shock is swept by, the test begins. The results of a typical computation for a nozzle area ratio of 11 is given in Figure 6. An analysis of this type becomes especially important when it is realized that for larger nozzle area ratios, the Q-shock might never detach from the throat under certain conditions.

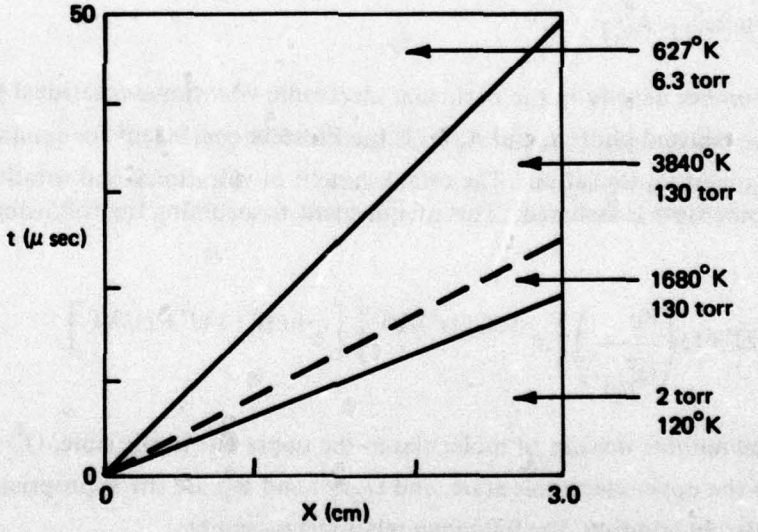

Figure 6. Wave Diagram Analysis for a Typical Experiment. Here the Area Ratio is 11 and the Test Gas is 3.4% $SnCl_4$ in Ar. The Reflected Shock Conditions were 6230°K and 5.1 Atm

During the course of these investigations, it was found that the thermal decomposition of $SnCl_4$ gives side products which are very efficient quenchers of the $SnO(a^3\Sigma^+)$ excited molecular state. To overcome this difficulty, an experiment was devised and successfully tested in which the tin vapor was furnished by the entrainment of the products of an exploding wire within the advancing shock wave. To accomplish this, a metal flange was equipped with high voltage electrodes which

permitted the placement of the tin wire parallel to the nozzle array and 1 inch upstream. The wire extends over the entire 12 inches of the plenum chamber. The energy to explode the wire was stored at high voltage (20 kV) in a 4μ Farad capacitor bank. The electrical noise was reduced to an acceptable minimum by housing the discharge circuit and capacitors in a metal housing and by isolating the data scope and attendant detection systems electrically by means of an isolation transformer. Typically, the wire was exploded 5 μsec before it was affected by the approaching shock wave. If the wire was exploded more than 15 μsec before shock arrival, the achievable number density was much reduced by loss of material to the walls. It did not prove possible to explode the wire after shock arrived due to its mechanical destruction.

The $SnCl_4$ and Sn wire used were purchased from Ventron in ultra pure (< 99%) and 99.999% purity levels respectively and were used without further purification. The N_2O and Argon used were purchased from Matheson with purities of 98% and 99.999% and used without purification.

2. CALIBRATIONS AND SPECTROSCOPY

Since the observation of chemiluminescence from SnO ($a \rightarrow X$) transitions has been the principal diagnostic during this investigation, a method of converting observed luminescent intensities to number densities of excited species is sought. We derive here the equations that permit the proper interpretation of the data.

The intensity of a spectral line in emission is given by

$$I = N^e_{v',J'}\, hc\omega^e_{v',J'}\, A^e_{v',J'} \tag{1}$$

Here $N^e_{v',J'}$ is the number density in the particular electronic-vibrational-rotational state, $\omega^e_{v',J'}$ is the wave number of the emitted photon, and $A^e_{v',J'}$ is the Einstein coefficient for spontaneous emission from the specified quantum transition. The establishment of vibrational and rotational equilibrium within each electronic state is assumed. This is equivalent to assuming the following relationship holds true [19]:

$$N^e_{v',J'} = (2J'+1)\left(\frac{\mu_o}{Q^e_{v',J'}}\right)\left[e^{-hcG_o(v')/kT}\right]\left[e^{-hcB^e_{v'}J'(J'+1)/kT}\right] \tag{2}$$

Here, μ_o is the total number density of molecules in the upper electronic state, $Q^e_{v',J'}$ is the partition function for the upper electronic state, and $G_o(v')$ and $B^e_{v'}$ are the appropriate vibrational and rotational constants. In addition, the following relationships apply:

$$A^e_{v',J'} = \frac{S(J',J'')}{\tau}\left[\frac{R^2_e(r)q(v',v'')}{\Sigma_{v''}R^2_e(r)q(v',v'')}\right] \tag{3}$$

Here, $S(J',J'')$ is the Honl-London factor. For $\Delta\Lambda = 0$, we have

$$S(J',J'') = J' \qquad \text{R-branch} \tag{4}$$

$$S(J',J'') = J'+1 \qquad \text{P-branch} \tag{5}$$

The term in brackets divided by the lifetime of the electronic state (τ) is the transition probability for the following process:

$$SnO\,(a^3\Sigma^+)_{v'} = SnO(X^1\Sigma^+)_{v''} \qquad (6)$$

The symbol q(v',v'') represents the Franck-Condon factor which is directly calculable [32]. For these calculations we assume τ = 333 μsec [7]. Finally, it is necessary to correct for the spectroscopic slit function, g($|\omega_{v',J'} - \omega_o|$, b c), which accounts for the fact that the spectrometer does not have infinite resolution. The functional dependence of g was determined by observing the apparent intensity distribution about the 6328Å line of a helium neon laser. The dependence observed is illustrated in Figure 7.

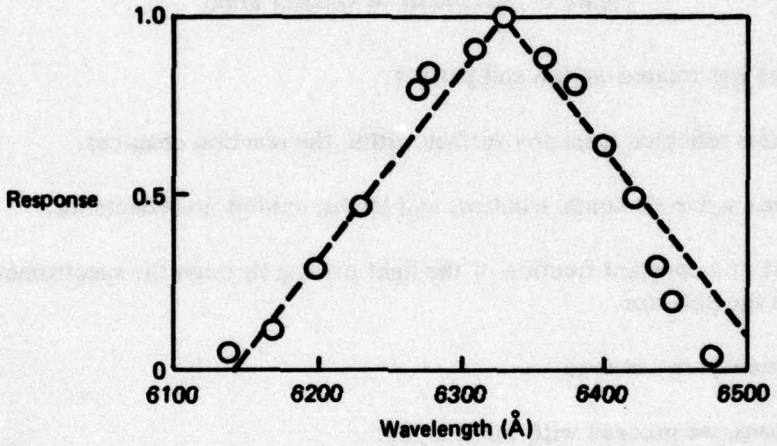

Figure 7. Spectral Response Curve Near 6328Å for 1/4 Meter Prism Monochromator for a Slit Width of 1.0 mm

The emission intensity per unit volume at wavelengths within the bounds of the slit function is given by

$$I = \Sigma_{v'}\Sigma_{J'} N^e_{v',J'} hc\omega_{v',J'} \frac{S(J',J'')}{\tau} \left[\frac{R_e^2(r)q(v',v'')}{\Sigma_{v''}R_e^2(r)q(v',v'')}\right] g(|\omega_{v',J'} - \omega_o|, b, c) \qquad (7)$$

The required absolute intensity measurements were made with the aid of a 1/4 meter prism monochromater. The spectroscopic slit function of the device was determined by use of a helium neon laser (0.5 mw) as the monochromatic source. The normalized results for a mechanical slit width of 1.0 mm are illustrated in Figure 7. The response curve was replaced by a triangular function having a half width of 190Å in all calculations, see the dashed line in Figure 7.

A brief description of the rationale and numerical analysis techniques used to quantitatively determine the amount of light reaching the detector from the extended source is in order. To accomplish this, we refer first to a schematic of the light train, see Figure 8. The following assumptions were made in the analysis to follow:

1. Except for apodization by the spectrometer slit and the circular outer diameter of the lens, the optical train was lossless.

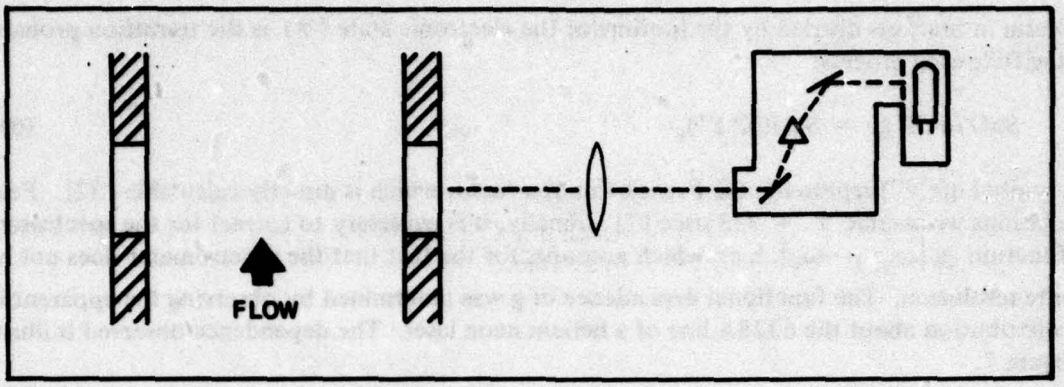

Figure 8. Schematic of Optical Train

2. The lens was treated as thin and perfect.

3. No light is reflected from any surface within the reaction chamber.

4. All transmissive elements, windows and lenses, exhibit no reflectance.

5. All light or a constant fraction of the light passing through the spectrometer slit reaches the detector.

6. All elements are centered.

With these assumptions, we proceed with the analysis.

The thin lens theory indicates that the position and size of the spectrometer slit as imaged by the lens is determined by the following relationships:

$$X' = f^2/X \tag{8}$$

and

$$m = X'/f \tag{9}$$

where

X = distance from slit to focal point of the lens
X′ = distance from image to back focus
m = magnification

It is clear that from any point in the luminous region a ray traveling through the open portion of the image of the slit so that it strikes within the clear aperture of the lens will be detected. The desired solution is then the total quantitative effect of all of these rays summed over the entire luminous region. This may be expressed mathematically as follows:

$$S_g = \iiint \Omega(X,Y,Z)dxdydz \tag{10}$$

where

Ω = the effective or open solid angle which reaches the detector at point (X,Y,Z) in the gas

dxdydz = incremental volume

A computer program was written which numerically approximates this integral by subdividing the luminous region into rectangular cells in a 3D mesh. At each cell in the mesh, the open or unobstructed solid angle as viewed from this point is determined, weighted by the volume of the cell, and summed. The solid angle elements are approximated by projecting the image of the slit onto the clear circular aperture of the lens as both would be viewed from the individual cell location. The common open area is determined and the solid angle approximated as follows:

$$\Delta\Omega_{ijk} \sim A_{ijk}/D^2_{ijk} \tag{11}$$

where

$\Delta\Omega_{ijk}$ = the open solid angle as viewed from the cell having coordinates (i,j,k)

A_{ijk} = common open areas in the plane of the lens

D_{ijk} = distance from the cell to the lens along a representative ray path.

Summation of these elements gives the desired result, i.e.,

$$S_g \sim \Sigma_i \Sigma_j \Sigma_k \, \Delta\Omega_{ijk} \Delta V_{ijk} \tag{12}$$

where

ΔV_{ijk} = the cell volume.

A slight complication is encountered when the slit is imaged within the luminous region. For points in the gas lying between the imaged slit and the lense, the projection of the image slit on the plane of the lens is determined by requiring the marginal rays defining the imaged slit to pass through the cell point.

After numerically computing the value of S_g, it is necessary to relate it to the chemiluminescent intensity of the gas. To do this, we first define the following parameters:

B_{chem} = Optical power radiated within the confines of spectral slit function into unit unit steradian solid angle per molecule $\equiv I/4\pi\mu_o$.

μ_o = The number density of radiating molecules.

V_T = Detector voltage recorded during the experiment.

V_c = Detector voltage measured when calibrating the device against the standard lamp.

I_{cal} = The manufacturer's standard lamp irradiance folded against the spectral slit function $g(|\omega_{v',J'} - \omega_o|, b, c)$.

D_{cal} = The distance quoted by the manufacturer in calibrating the lamp.

T_F = The transmittance of any neutral density filters used during calibration of the lamp.

S_g = Integrated effective solid angle volume product of the luminous gas.

D^*_{cal} = Actual distance of the calibration lamp from the imaged slit.

h = Slit height.

W = Slit width.

K = Proportionality constant.

I_ω = The manufacturers standard lamp irradiance density at frequency ω (cm^{-1}).

If the distance from the standard lamp is great enough to assure that its brightness is the same as an equivalent point source, we have

$$B_{cal} \sim I_{cal} \cdot D^2_{cal} \ |\text{watts/steradian}| \tag{13}$$

The detector voltage recorded during calibration will be

$$V_c = KB_{cal} \cdot (hwm^2) T_F / (D^*_{cal})^2 \tag{14}$$

Similarly, for the shock tube experiment,

$$V_T = KB_{chem} \cdot \mu_o \cdot S_g \tag{15}$$

When the proportionality factor, K, is eliminated from these two expressions, we obtain

$$B_{chem} = V_T \left[\frac{T_F I_{cal} hwm^2 D^2_{cal}}{S_g \mu_o V_c (D^*_{cal})^2} \right] \tag{16}$$

When the definition for B_{chem} is substituted into this expression, the following expression is obtained:

$$I = V_T \left[\frac{4\pi I_{cal} hwm^2 D^2_{cal}}{S_g V_c (D^*_{cal})^2} \right] \tag{17}$$

$$= V_T C$$

where

$$C = 4\pi T_{cal} hwm^2 / S_g V_c (D^*_{cal}/D_{cal})^2 \tag{18}$$

For the conditions of our experiment, we estimate the value of S_g at 0.028 steradian-cm^3. In estimating the value of this parameter, the effects of surface reflections were neglected. If included, these effects would tend to lower the computed value of C and ultimately of μ_o.

The standard lamp was a quartz-iodine 1000 watt device which was calibrated against an NBS standard. The calibration curve is given in Figure 9. Also, we have the following values:

h = 2 cm

w = 0.1 cm

m = 0.5

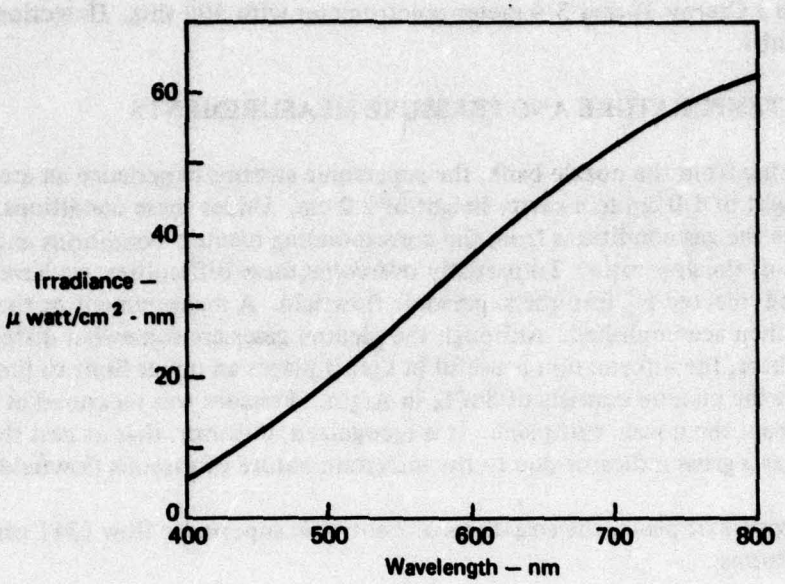

Figure 9. Spectral Irradiance of the Standard Lamp as a Function of Wavelength at a Distance of 30 cm and Operated at 8.3 Amperes

D^*_{cal} = 11.25 cm

D_{cal} = 30 cm

V_c = 0.34 volts

$I_{cal} = \int_{\Delta\omega} I_\omega g(|\omega_{v',J'} - \omega_o|, b, c)\, d\omega = 543\ \mu watt/cm^2$

T_F = 0.01

With these values, the following result is obtained:

$$I = 2.55 \times 10^{-3}\ V_T \text{ watts}$$

The solution of equation (7) for I at 1000°K gives the following result for a spectrometer setting of 5544Å:

$$I/\mu_o = 0.48 \times 10^{-16} \text{ watts}$$

From these two expressions, we obtain the desired result, i.e.,

$$\mu_o = 5.3 \times 10^{13}\ V_T \text{ molecules/cc}$$

Since we have used the same optical arrangement throughout this investigation, this expression is applicable so long as the cavity temperature is 1000°K.

Finally, it was initially hoped that the densities of atomic tin states could be monitored by atomic resonance absorption measurements. It was found, however, that when the source material was shock-heated $SnCl_4$ in Argon intense resonance line emission was observed at all of the characteristic Sn atom frequencies. As a consequence, the presence of Sn vapor in the flowfield was established by monitoring the emission at 3802Å from the $Sn(6^3P_1 \rightarrow 5^1D_2)$ resonance line. Spectral

isolation was with a Czerny Turner 3/4 meter spectrometer with 30μ slits. Detection was by means of a 1P28 phototube.

3. CAVITY TEMPERATURE AND PRESSURE MEASUREMENTS

Upon exiting from the nozzle bank, the supersonic streams experience an area step function from a nozzle height of 1.0 cm to a cavity height of 2.2 cm. Under these conditions, it is difficult at best to estimate the gas conditions from the corresponding plenum conditions and the dimensional parameters of the apparatus. To partially overcome these difficulties, we have a plenum of Argon with F_2 and injected H_2 into the supersonic flowfield. A measurement of the HF rotational temperature was then accomplished. Although the plenum gases are somewhat different than those under discussion here, the information is useful in that it places an upper limit to the temperature to be expected when the plenum consists of $SnCl_4$ in Argon. Pressure was measured at the wall a distance of 2.5 cm from the nozzle exit plane. It is recognized, however, that at best this measurement can be used only as a gross indicator due to the uncertain nature of gaseous flowfield.

At the nozzle exit plane, the equations of isentropic supersonic flow [31] can be expressed by the following forms:

$$\Gamma = C_w O_o A_t \left(\frac{1}{RT_oM}\right)^{1/2} \sqrt{\gamma\left(\frac{2}{\gamma+1}\right)^{(\gamma+1)/(\gamma-1)}} \tag{19}$$

$$P_c/P_o = 1\Big/\left[1+\frac{\gamma-1}{2}M^2\right]^{\gamma/(\gamma-1)} \tag{20}$$

$$T_c/T_o = 1\Big/\left[1+\frac{\gamma-1}{2}M^2\right] \tag{21}$$

$$\frac{A}{A^*} = \frac{1}{M}\left[\frac{2}{\gamma+1}\left(1+\frac{\gamma-1}{2}M^2\right)\right]^{\frac{\gamma+1}{2(\gamma-1)}} \tag{22}$$

The symbols have the following meanings:

- Γ = the molar flow rate of plenum gases into the cavity,
- C_w = the nozzle discharge coefficient (assumed unity here),
- P_o = the plenum pressure,
- A^* = the effective throat cross-sectional area (assumed equal to A_t),
- R = the gas constant
- T_o = the plenum temperature
- γ = the heat capacity ratio (1.667),
- A = the exit plane dimension
- M = the gas Mach no.
- A_t = the geometric throat area.

With these equations, it is possible to place upper limits to the values of Γ, P_c, and T_c.

Typically the HF rotational temperature was determined by simultaneously monitoring the intensities of the $R^{2\rightarrow0}$ (6) and $R^{2\rightarrow0}$ (1) rotational lines centered at 12576.9Å and 12780.8Å respectively. Spectral isolation was by means of a 3/4 meter Czerny Turner monochrometer equipped with a polychromator attachment. Detection was by means of two Ge chip detectors which were calibrated by comparison to a standard blockbody source. Typical results of these measurements are given in comparison to the values computed for simple isentropic flow in Table IV. As can be seen from the comparison given, the computed values appear to be a reasonable approximation to the measured values for the temperature; whereas, an uncertainty of about a factor of two exists for the pressure. Before experimental results can be compared to the model calculations, Section I-2, with maximum confidence, it will be necessary to better characterize these pressure measurements. Our intent is to measure the free stream number density with an interferometer.

TABLE IV
HF ROTATIONAL TEMPERATURES AND MEASURED WALL PRESSURES AS COMPARED TO THE IDEAL ISENTROPIC VALUES FOR TYPICAL EXPERIMENTAL CONDITIONS

				Measured Values		Isentropic Values*	
$\%SnCl_4$	$\%F_2$	T_o °K	P_o (atm)	T_c °K	P_w (torr)	T_c °K	P_c (torr)
0	10	7050	8.1	700 ± 100		691	19.0
0	3	10400	10.7	1080 ± 100		1020	22.0
3.3	0	6850	3.7		5 ± 1		8.5
3.3	0	7830	4.2		5 ± 1		9.6
2.3	0	7200	2.9		6 ± 1		6.6

*Computed for an area ratio of 11 at the nozzle exit plane.

III. RESULTS AND DISCUSSION

1. TIN ATOM DETECTION

A typical oscillogram showing the Sn atom emission intensity and the accompanying cavity pressure trace is illustrated in Figure 10. An entire series of these tests was conducted with only the percentage of $SnCl_4$ in the initial mix varying from test to test. The peak intensity of these traces is shown as a function of the percentage of $SnCl_4$ in the initial plenum mix in Figure 11. When the wavelength selector is set 10Å to either side of a resonance line, no emission is observed by the phototube.

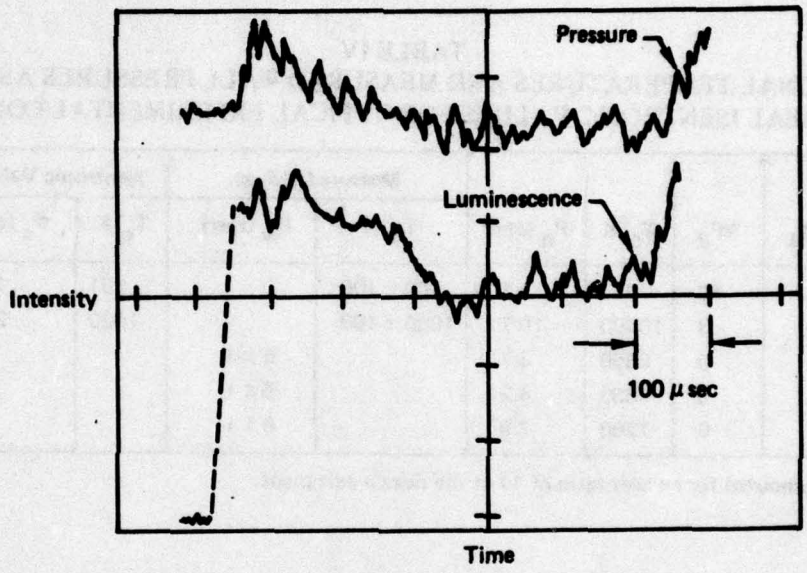

Figure 10. Oscillogram Illustrating the Sn Atom Luminescent Intensity and Cavity Pressure for 0.8% $SnCl_4$ in Argon Shock Heated to 10,000°K and 4.0 Atm. Nozzle Area Ratio was 11. Cavity Temperature ~ 1015°K

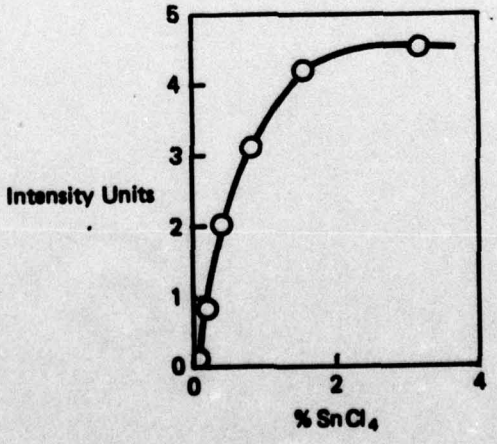

Figure 11. Effect of Sn Density Upon the Resonant Line Emission Intensity at 3801Å. Reflected Shock Conditions of 9700 ±900°K and 4.0 ± 0.6 Atm Respectively

It would appear from these results that the radiant intensity follows the cavity pressure closely and is a nonlinear function of the tin atom density. Furthermore, since the resonant transition is allowed in electric dipole theory, it is likely that the radiation has its origin in a chemical process. This follows directly from the fact that approximately 20 μsec are required for a gas particle to transit the nozzle and appear in the field of view. Since the radiative lifetime of the 6^3P_1 state is only 67 n sec, all radiation of a thermal origin will be lost [33]. A possible mechanism for this effect is as follows:

$$\begin{aligned} Sn + Cl + M &= SnCl^* + M \\ SnCl^* + Sn &= SnCl + Sn^* \\ Sn^* + M &= Sn + M \end{aligned} \qquad (23)$$

The asymptotic approach to an upper limit is indicative of an efficient quenching of the 6^3P_1 state by a product molecule, possibly Sn or Cl. In the case of the exploding wire, this tin atom resonant emission was not observed. This is a further indication of the chemical nature of the effect.

In the absence of a suitable resonance absorption technique, at least for the case of $SnCl_4$ dissociation, we have utilized a measurement of the resonance intensity at 3802Å as a simple indicator to establish the presence of Sn vapor in the cavity. In order to give a more quantitative aspect to the results, we have resorted to a titrametric procedure to be described later under the heading of the exploding wire.

2. TIN TETRACHLORIDE VAPOR SOURCE

A typical oscillogram showing the SnO ($a^3\Sigma^+ \rightarrow X^1\Sigma^+$) emission centered at 5544 ± 90Å is shown in Figure 12. An entire series of these tests was conducted with only the percentage of $SnCl_4$ in the initial mix being changed. The steady state intensity of the resulting traces is shown as a function of the percentage of the $SnCl_4$ in the initial plenum mix in Figure 13.

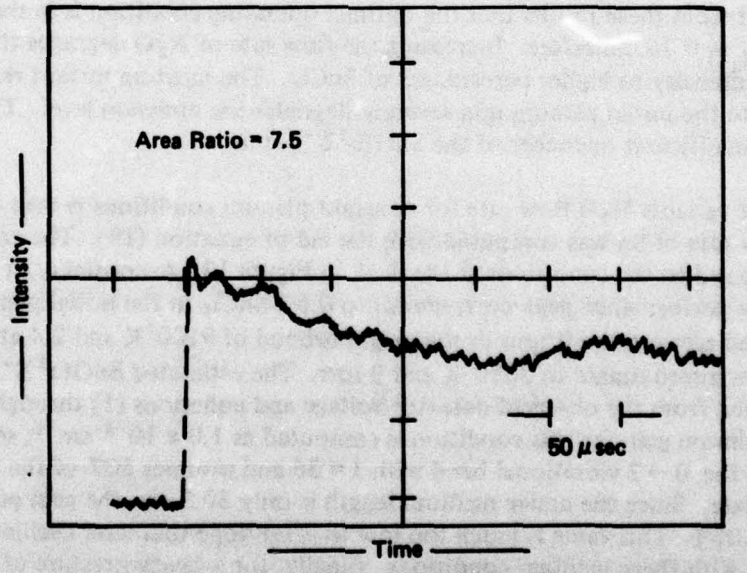

Figure 12. Oscillogram Illustrating the a → X Emission from SnO Centered at 5544 ± 90Å. Plenum Conditions were 9675°K and 2.4 Atm. Estimated Cavity Conditions were 1146°K and 8.7 torr with $X_{Sn} = 0.0015$ and $\dot{n}_{Sn}/\dot{n}_{N_2O} \sim 0.045$

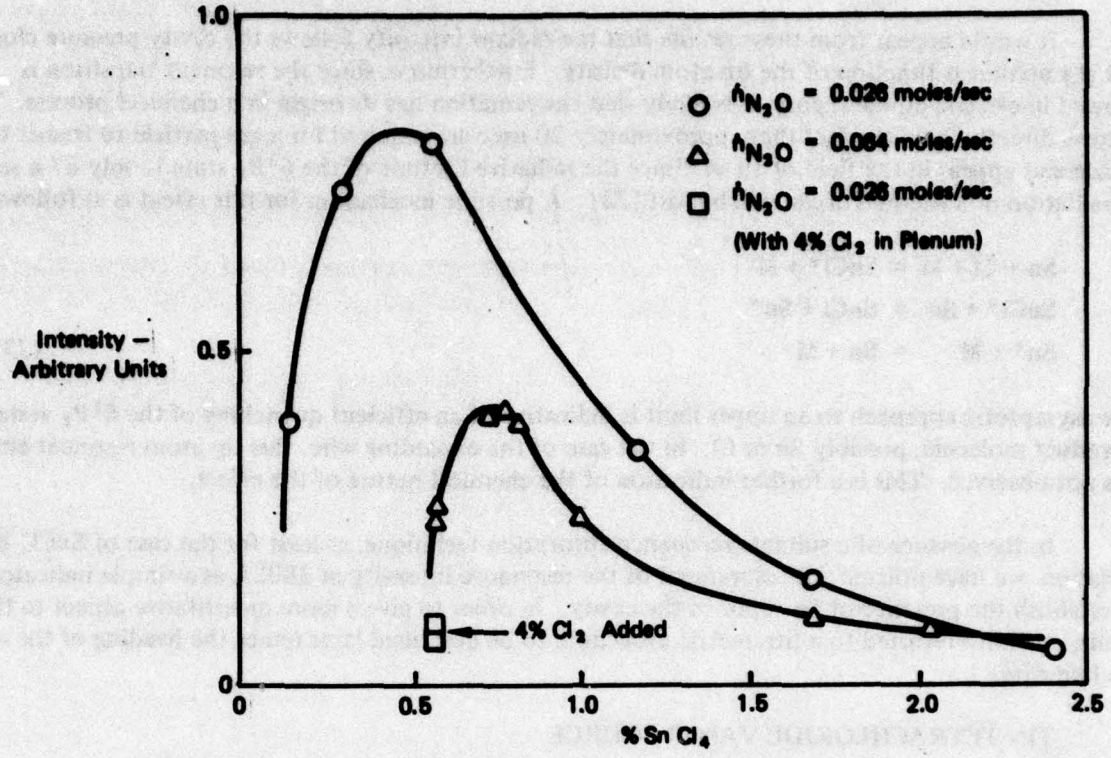

Figure 13. Intensity of Emission at 5544 ± 90Å as a Function of Initial $SnCl_4$ Partial Pressure. The Plenum Conditions Varied from 9675°K and 2.4 Atm at 0.15% to 7140°K and 2.5 Atm for 2.5%. Corresponding Cavity Temperatures were 1146°K and 846°K. Effect of N_2O Flow Rate and of Added Cl_2 are Also Shown.

It is apparent from these results that the optimal operating condition is in the neighborhood of 0.6% $SnCl_4$ with $\dot{n}_{N_2O}$ 0.26 moles/sec. Increasing the flow rate of N_2O degrades the performance and shifts the peak intensity to higher percentages of $SnCl_4$. The most important result here is that the addition of Cl_2 to the initial plenum mix severely degrades the emission level. The conclusion here is that atomic Cl is an efficient quencher of the $SnO(a^3\Sigma^+)$ state.

The effect of variable N_2O flow rate for constant plenum conditions is seen more clearly in Figure 14. The flow rate of Sn was computed with the aid of equation (19). The conditions for peak performance correspond to the conditions at the peak in Figure 13. Accordingly, it would appear from these results that the performance peak corresponds to 0.6% $SnCl_4$ in the initial plenum mix with $\dot{n}_{N_2O}/\dot{n}_{Sn} \sim 2.5$ and plenum conditions in the neighborhood of 9100°K and 2.4 atm. The corresponding cavity conditions approximate to 2080°K and 9 torr. The estimated $SnO(a^3\Sigma^+)$ density for these conditions as obtained from the observed detector voltage and equations (1) through (18) is 7×10^{-11} moles/cc. The maximum gain for this condition is computed as 1.0×10^{-5} cm^{-1}, see equation (xi). This corresponds to the $0 \rightarrow 3$ vibrational band with J = 36 and assumes 50% of the SnO to be in the ground electronic state. Since the active medium length is only 30.5 cm, the gain per pass that is achievable is only 0.03%. This value is much too low to offer hope that laser oscillations can be induced in a real laser cavity with these medium conditions. Finally, for a cavity pressure of 9 torr at 1080°K, the total SnO density for 0.6% $SnCl_4$ in the initial mix will be 8×10^{-10} moles/cc. This result suggests that for a Sn vapor source which utilizes $SnCl_4$, over 90% of the SnO present in the active medium is in the ground state even under the most optimum conditions. To overcome these difficulties, an alter-

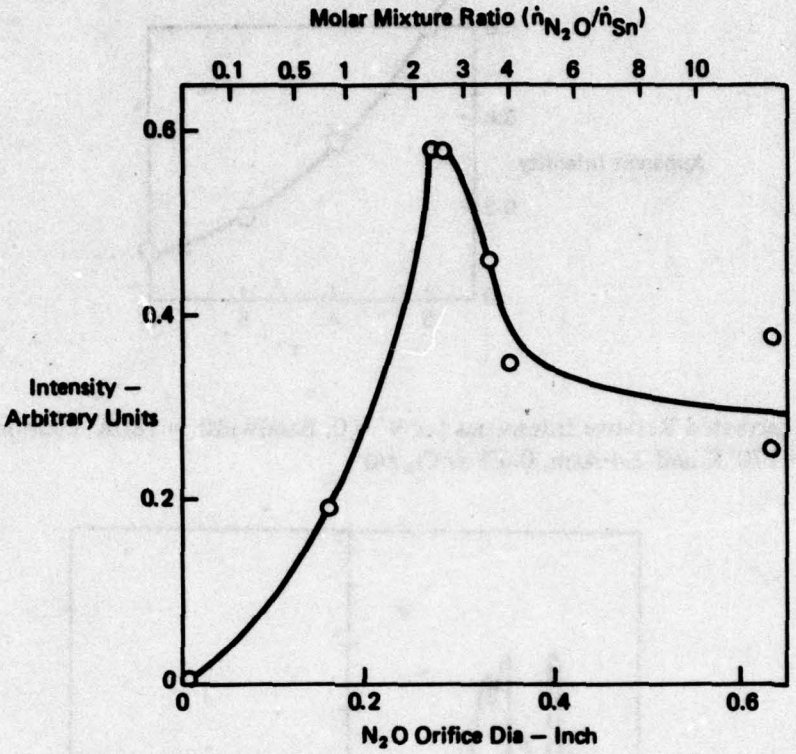

Figure 14. Effect of N_2O Flow Rate Upon Emission Intensity at 5544 ± 90Å. The Plenum Conditions Correspond to 9120 ± 200°K and 2.4 ± 0.1 Atm. Estimated Cavity Temperature was 1080 ± 30°K

nate source of Sn vapor must be utilized. This alternate source should not introduce undesirable by-products into the flowfield. We have selected the use of an exploding wire technique to be explained below.

Finally, tests were conducted for which one of the two reactants were absented from the flowfield. When this is done, no emission is observed in the range 5544 ± 90Å, although, if Sn is present the resonant line emission is present. In addition, the relative intensities of several bands in the $a \rightarrow X$ manifold have been measured. The data, uncorrected for variable detector response, is given in Figure 15. As is to be expected, maximum intensity is obtained when the wavelength selector is tuned to a vibrational band.

3. EXPLODING WIRE TECHNIQUE

A typical oscillogram showing the SnO ($a^3\Sigma^+ \rightarrow X^1\Sigma^+$) emission centered at 5544 ± 90Å is shown in Figure 16. In these tests, the plenum was always argon with entrained wire products. Typically, the cavity conditions will be approximated by 1145°K and 8.7 torr. These figures do not account for the wire discharge energy which is coupled into the gas. The unfortunate feature of these tests is the small useful test time (7 ~ 100 μsec). Nevertheless, a substantial increase in peak radiant intensity is observed (improvement of more than an order of magnitude) relative to the use of $SnCl_4$. When no N_2O is flowed, no emission, including the initial spikes, is observed at the stated wavelength.

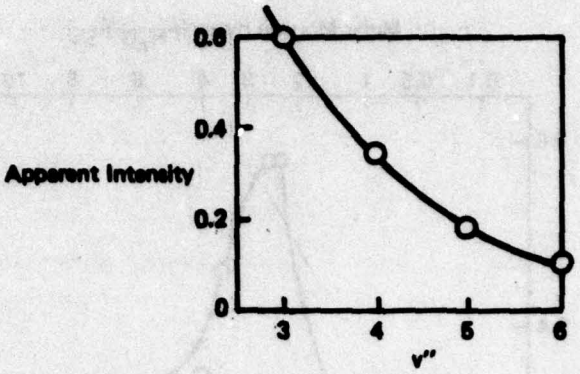

Figure 15. Uncorrected Relative Intensities for V' = 0, Bandwidth = 180Å, Plenum Conditions of 9170°K and 2.4 Atm, 0.6% $SnCl_4$/Ar

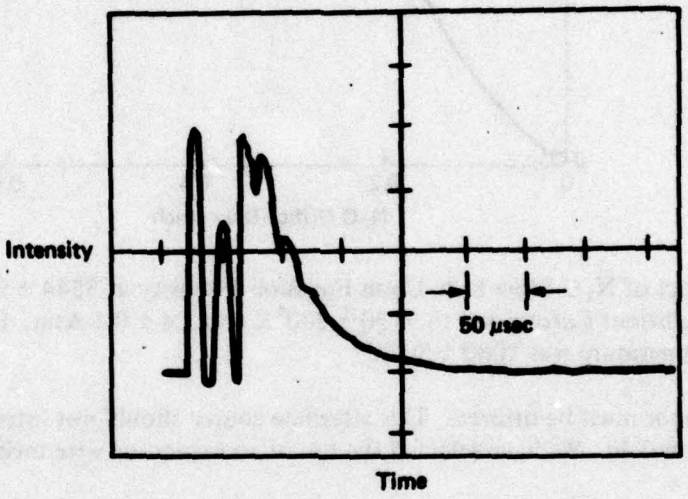

Figure 16. Oscillogram Showing Chemiluminescent Intensity at 5544 ± 90Å with Plenum Conditions of 9660°K and 2.3 Atm. A 0.25 Dia. Wire was Exploded at 800 Joules $\dot{n}/_{N_2O}$ = 0.0113 moles/sec

The effect of discharge energy upon the radiant intensity is shown in Figure 17. The peak intensity observed corresponds to a SnO ($a^3\Sigma^+$) density of 2.2×10^{-9} moles/cc. This corresponds to an achievable gain of approximately 1.6×10^{-4} cm^{-1}. For the single pass medium length of 30.5 cm, this corresponds to a total gain of 0.48% per pass. This is approaching the region of interest for lasing.

We estimate from the estimated plenum conditions that approximately 3.6% of the gas will be molecular SnO when the discharge energy is 1200 joules. This assumes that approximately 50% of the SnO is in the ground electronic state.

A simple titration of the Sn vapor with N_2O is illustrated in Figure 18. Although the data appear to be approaching an asymptotic limit, the initial rise is so sharply differentiated from data at higher flow rates that it is tempting to assume that the stoichiometry is balanced at approximately 0.03 moles of N_2O per second. This assuamption is, however, not justified due to the slow reaction rate. A

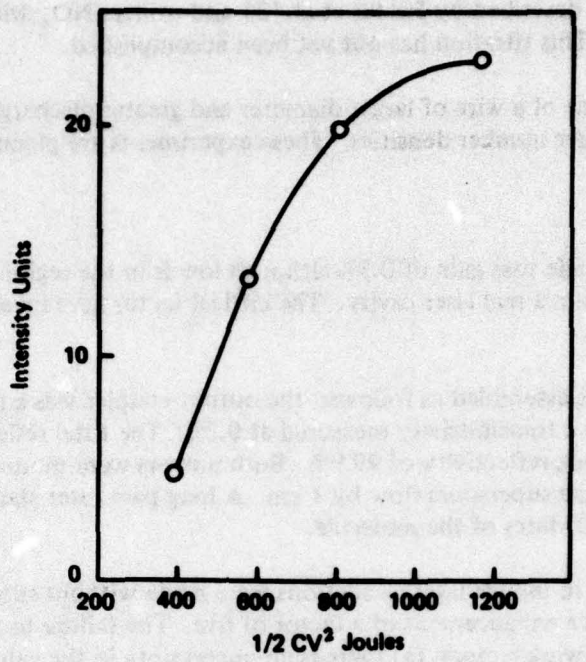

Figure 17. Illustration of Dependence of Radiant Intensity at 5544 ± 90Å Upon Wire Discharge Energy. Plenum Conditions were 9650 ± 100°K and 2.3 ± 0.1 Atm. $\dot{n}_{N_2O}$ = 0.13 moles/sec

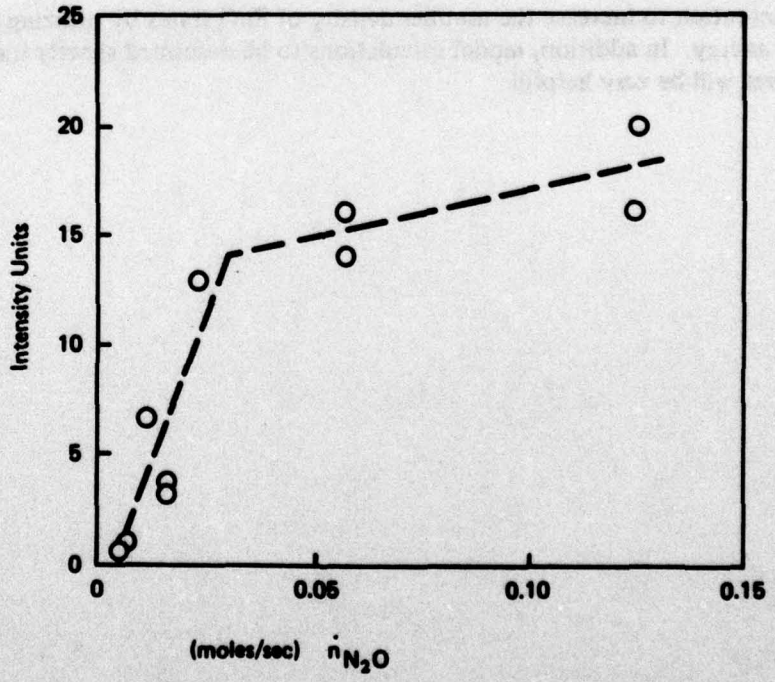

Figure 18. Illustration of Functional Dependence of Radiant Intensity at 5544 ±Å Upon Flow Rate of N_2O. Plenum Conditions were 9650 ± 100°K and 2.3 ± 0.1 Atm. Discharge Energy was 800 Joules

better titration has been described by Felder et al. [3] and utilizes NO_2 which reacts with Sn vapor much more efficiently. This titration has not yet been accomplished.

It is likely that use of a wire of larger diameter and greater discharge energy will permit the achievement of even higher number densities. These experiments are planned for the future.

4. LASER TESTS

The estimated single pass gain of 0.5% although low is in the region that might permit the inducement of laser oscillations in a real laser cavity. The critical factor here involves the use of mirrors of very high reflectivity.

A laser cavity was assembled as follows: the output coupler was a dielectric flat with a peak reflectivity of 99.7% and a transmissivity measured at 0.2%. The total reflector had a radius of curvature of 2 meters and a peak reflectivity of 99.9%. Both mirrors were mounted internally to the windows but were recessed from the supersonic flow by 1 cm. A long pass filter starting at 5500Å blocked contributions from the b and D states of the molecule.

Several attempts to induce laser oscillations were made without success. The mirrors, when aligned, do give a radiative enhancement of a factor of five. The failure to induce oscillations is probably due to either of the following factors: (a) there is an uncertainty in the value of the electronic transition moment [7]. This uncertainty amounts to at least a factor of 3. We have used the most optimum value, $7 \sim 333$ μsec. (b) there is always uncertainty in the stated reflectivities of commercial mirrors. We have assembled a cavity with a single pass mirror loss of 0.4%. When considered in view of the estimated single pass gain, there is not much margin for error.

It is our intention to increase the number density of SnO states by utilizing a heavier wire and greater discharge energy. In addition, model calculations to be described shortly indicate that lower cavity temperatures will be very helpful.

IV. MODEL CALCULATIONS AND CONCLUSIONS

The computer model has been used to begin mapping the gain regions for the system in an effort to better guide the experimental effort in the future. Some of the more interesting results to date are illustrated in Figures 19 and 20. It would appear from these results alone that the laser cavity experiments conducted to date were done at much too high a cavity temperature. These calculations were all done with the assumption of a laminar diffusive mixing of the two flow streams. This approach gives the least optimistic result.

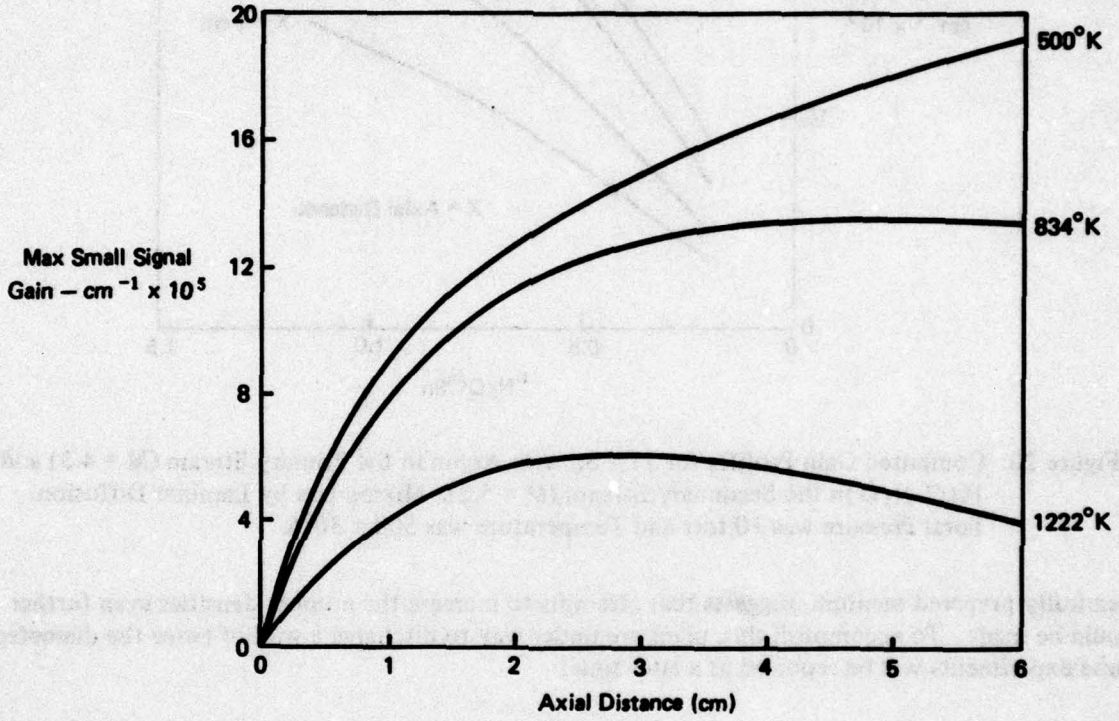

Figure 19. Computed Gain Profiles for 11% Sn with Argon in the Primary Stream (M = 4.3) and 100% N_2O in the Secondary Stream (M = 5.2). Mixing is by Laminar Diffusion. Total Pressure is 10 torr with $\dot{n}_{N_2O}/\dot{n}_{Sn}$ = 2.8 on a Molar Basis

The effect of N_2O concentration and axial position are illustrated in Figure 20. It is apparent from these results that the 2.5 cm position of the current optical axis is too close to the injector. In addition, if optimum gain is to be achieved, it will be necessary to increase the N_2O flow rate beyond what can now be achieved in the apparatus as depicted in the figure. The maximum N_2O flow rate that can now be achieved is approximately 0.13 moles/sec. This corresponds to the upper limit shown on the abscissae of the figure.

Finally, the quantitative aspects of the data, Figure 18, are well reproduced by the model calculations, Figure 20. Once the gas density within the laser cavity has been better characterized, the quantitative comparison will be made. For the present, however, the semiquantitative comparisons which have been made suggest that the number densities of excited states that have been achieved are approaching the region of interest. This, coupled to the failure to induce laser oscillations in the

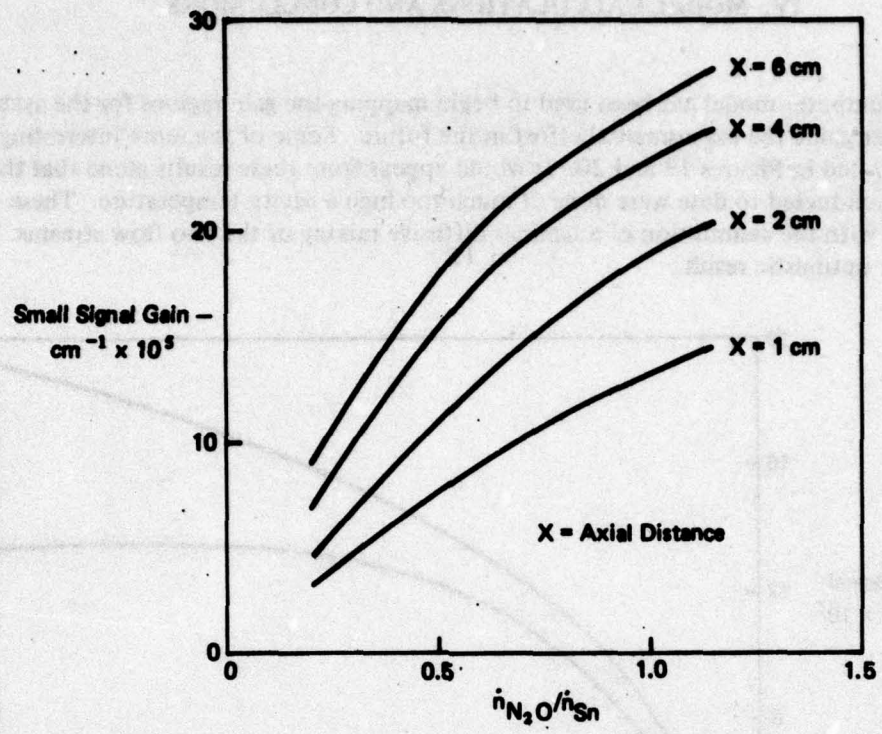

Figure 20. Computed Gain Profiles for 11% Sn with Argon in the Primary Stream (M = 4.3) and 100% N_2O in the Secondary Stream (M = 5.2). Mixing was by Laminar Diffusion. Total Pressure was 10 torr and Temperature was 500 ± 30°K

chemically prepared medium, suggests that attempts to increase the number densities even further should be made. To accomplish this, plans are under way to discharge a wire of twice the diameter. These experiments will be reported at a later time.

V. REFERENCES

1. Eckstrom, D.J., Edelstein, S.A., and Benson, S.W., J. Chem. Phys., 60, 2930 (1974).

2. Obenauf, R.H., Hsu, C.J., and Palmer, H.B., J. Chem. Phys., 58, 4693 (1973).

3. Felder, W.H. and Fontijn, A., J. Chem. Phys., 69(3), 1112 (1978).

4. M.J.Linevsky and R.A. Carabetta, "Chemical Laser Systems," Final Report, Contract F29601-76-C-0055, May 1977.

5. Gole, J.L., Elect. Trans. Lasers, II, 136 (1976).

6. Fischell, D.R., and Cool, T.A., Elect. Trans. Lasers, II, 166 (1976).

7. Suchard, S.N., "Spectroscopic Constants for Selected Diatomic Molecules," SAMSO-TR-74-82, March 1974.

8. Armstrong, R. and Davis, S., Elect. Trans. Lasers, II, 133 (1976).

9. Betts, J.A., and Miller, D.J., Elect. Trans. Lasers, II, 198 (1976).

10. Cadman, P. and Polanyi, J.C., J. Phys. Chem.. 72, 3715 (1968).

11. Blauer, J.A., Janiak, D., and Solomon, W.C., Elect. Trans. Lasers, II, 283 (1976).

12. Herbelin, J.M., Kwok, M.A., and Spencer, D.J., Elect. Trans. Lasers, II, 96-106 (1976).

13. Pritt, A.T. Jr., Coombe, R.D., Phillipovich, D., Wagner, R.I., Bernard, D., and Dymek, C., Appl. Phys., Lett., 31, 745 (1977).

14. Oldenborg, R., Dickson, C., and Zare, R.J., Molec. Spectr., 58, 283 (1975).

15. Hall, L.H., IEEE J. Quant. Electr., II, 693 (1975).

16. Steinberg, M. and Kudryoutsev, Y.M., Univ. or Calif., Final Rept., Contract No. DAAH01-75-C-0339, 1976.

17. Capelle, G.A. and Brown, J.M. Jr., Elect. Trans. Lasers, II, 56-59 (1974).

18. McDermott, W.E., Pchelkin, N.R., Benard, D.J., and Bousek, R.R., Appl. Phys. Lett, 32(8), 469-70 (1978).

19. Hertzberg, G., "Molecular Spectra and Molecular Structure: I. Spectra of Diatomic Molecules," pp. 390-399, Van Nostrand Reinhold Co., New York, 1950.

20. Herzfeld, K.F., and Litovitz, T.A., "Absorption and Dispersion of Ultrasonic Waves," pp. 285-299, Academic Press, Inc., New York, 1959.

21. Blair, R., Johnson, S.E., and Watson, G.W., Xonics Tech. Rept. TR-54 (1975).

22. Wiesenfeld, J.R. and Yuen, Chem. Phys. Letters, 42, 293 (1976).

23. Capelle, G.A. and Linton, C., J. Chem. Phys, 65, 5361 (1976).

24. Procaccia, I. and Levine, R.D., J. Chem. Phys., 63, 4261 (1975).

25. Benson, S.W. and Fueno, T., J. Chem. Phys., 36, 1597 (1962).

26. Keck, J. and Kalelkar, A., J. Chem. Phys., 49, 3211 (1968).

27. Benson, S.W., "Thermochemical Kinetics," pp 148-200, John Wiley and Sons, New York, 1976.

28. Hampson, R.F. and Garvin, "Reaction Rate and Photochemical Data for Atmospheric Chemistry," NBC Special Publication 513, 1977.

29. Brown, A. and Husain, D., J. Less Common Metals, 3, 305 (1974).

30. Felder, W.H. and Fontijn, A., "Kinetics and Spectroscopy of the Sn/N_2 O Electronic Transsition Chemical Laser Candidate Reaction," AFWL-TR-76-162, 1976.

31. Rudinger, George, "Nonsteady Duct Flow and Wave-Diagram Analysis," pp 163-68, Dover Publications, Inc., New York, 1969.

32. Lillis, J.R. and Harris, R.A., Franck-Condon Factors and Relative Intensities for the SnO SnO($a^3\Sigma - X^1\Sigma$) and SnO($b^3\pi - X^1\Sigma$) Band Systems," AFWL-TR-74-344, Fall 1974.

33. Lawrence, G.M., Astrophys, J., 148, 261-8 (1976).